PTEP

Prog. Theor. Exp. Phys. **2022** 043F01(11 pages)
DOI: 10.1093/ptep/ptac016

A new semi-empirical model for cosmic ray muon flux estimation

Junghyun Bae* and Stylianos Chatzidakis

School of Nuclear Engineering, Purdue University, West Lafayette IN 47906, USA

*E-mail: bae43@purdue.edu

Received November 6, 2021; Revised January 4, 2022; Accepted January 25, 2022; Published January 31, 2022

Cosmic ray muons have emerged as a non-conventional high-energy radiation probe to monitor dense and large objects. Muons are the most abundant cosmic radiation on Earth; however, their flux at sea level is approximately $10^4\ \mathrm{min}^{-1}\mathrm{m}^{-2}$, much less than that of induced radiation. In addition, cosmic ray muon flux depends on not only various natural conditions, e.g., zenith angle, altitude, or solar activity, but also the geometric characteristics of detectors. Since the low muon flux typically results in long measurement times, an accurate estimation of measurable muon counts is important to improve the efficiency of muon applications. Here we propose a simple and versatile semi-empirical model to improve the accuracy in muon flux estimation at all zenith angles by incorporating the geometric parameters of detectors, and we name this the 'effective solid angle model.' To demonstrate the functionality of our model, it is compared with (i) the cosine-squared model, (ii) the PARMA model, (iii) Monte Carlo simulations, and (iv) experimental measurements. Our results show that the muon count rate estimation capability is significantly improved, resulting in increasing a mean C/E level from 0.7 to 0.95. In addition, by selecting an appropriate intensity correlation, the model can be easily extended to estimate muon flux at various altitudes and also underground.

Subject Index E41, F00, F40, F43

1. Introduction

Cosmic ray muons account for the major portion of cosmic radiation reaching Earth [1]. Due to their high-energy and penetrating nature, cosmic ray muons have been proposed as a non-conventional radiation probe for imaging and monitoring high-Z, large, and dense objects, typically a challenge with conventional radiography techniques. Specifically, muon applications have been studied in many fields, e.g., spent nuclear fuel cask and reactor imaging [2–8], homeland security [9–16], and geotomography [17–20]. Despite efforts to further maximize the utilizability of cosmic ray muons [21–24], their applicability is often limited by the naturally low flux at sea level (about 10^4 muons per minute per m^2) and its large variance with zenith angle. Cosmic muons are mainly produced by pion decays at an altitude of approximately 15 km. The measurable cosmic ray muon flux highly depends on the muon's traveling distance because it decays to electrons/positrons with a mean lifetime of 2.2 μsec and is attenuated in the Earth's atmosphere. One widely used empirical model for the relationship between cosmic particle flux and zenith angle, φ, is the cosine-power model. For cosmic ray muons at sea level, the exponent of cosine-power model is approximated to 2, or $I(\varphi) = I_0 \cos^2\varphi$ [25]. However, the cosine-squared model is limited due to its detector geometry assumption of a point detector. For example, according to the cosine-squared approximation, no muon will be detected in the horizonatal direction ($\varphi = 90^\mathrm{o}$) regardless of a detector size or configuration. However, cosmic muons can be measured at any zenith angle and there exist radiographic techniques using horizontal muon detectors [26,27]. Although accurate analytical models for terrestrial cosmic ray flux estimation have been developed [28–30], detector geometry and configuration are not taken into account in these models. To address this gap, we aim to develop a new model that can easily estimate the expected cosmic muon count rates at all zenith angles at sea level for use in various engineering applications.

In most muon applications including muon radiography and monitoring, at least two-fold coincidence muon detectors are installed and the target objects are placed between two detectors. According to the cosine-squared model, the expected muon counts only depend on the active surface area of the detectors. However, they also depend on the distance between the two detectors because their measurable solid angle becomes larger as the distance decreases. To consider the geometry and configuration of detectors in cosmic muon flux estimation, we developed a new approach named the effective solid angle. To demonstrate the performance of effective solid angle model, we design and perform cosmic ray muon experiments and Monte Carlo simulations. The experimental and simulation results are compared with both empirical and analytical estimations: cosine-squared, the PARMA model [29], and effective solid angle models.

Another way to improve the cosine-squared model focuses on finding a better estimation for the cosine power (instead of 2) [31,32]. However, none of them provides a solution to the large uncertainties in high zenith angles using either a cosine-power or -squared model. For muon applications, data acquisition and statistics are essential processes because they determine the quality of outcomes. Hence, the effective solid angle model can play an important role in estimating the necessary measurement time or volume of muon data to achieve the expected outcomes with small uncertainty in all zenith angles. In the end, we present the effective solid angle equations that can be universally applied in all detector configurations and zenith angles. In addition, a semi-empirical equation is included so that the computed effective solid angle is converted to muon count rates.

2. Semi-empirical effective solid angle model

Although the centerline of a detection system is aligned with the vertical direction, $\varphi = 0^\mathrm{o}$, it will not only detect muons that arrive at 0^o zenith angle. Due to the finite size of detector systems, some muons with $\varphi \neq 0^\mathrm{o}$ can be detected. Similarly, even though the centerline of a detection system is aligned with the horizontal direction, $\varphi = 90^\mathrm{o}$, some muons are still detected because not all muons come from the horizontal direction. Therefore, both the detector geometry and distance between two detectors must be considered when estimating the muon flux.

The effective solid angle depends on both a size and distance of two detectors, and also it continuously varies on the detector surface as shown in Fig. 1 (left). Because the muon flux variance along the azimuthal angle is insignificant [33], the solid angle only depends on a distance from the detector centerline on the surface. An example of the approximated solid angle at a point P (red) which is distant from the centerline with a radius, r, and the detector distance, D, is shown in Fig. 1 (right). To compute the effective solid angle, we find the projected plane angle, θ, which is a two-dimensional angle at point P. The projected plane angle is a function of r, however it is independent of the height (or thickness) of detector under the assumption

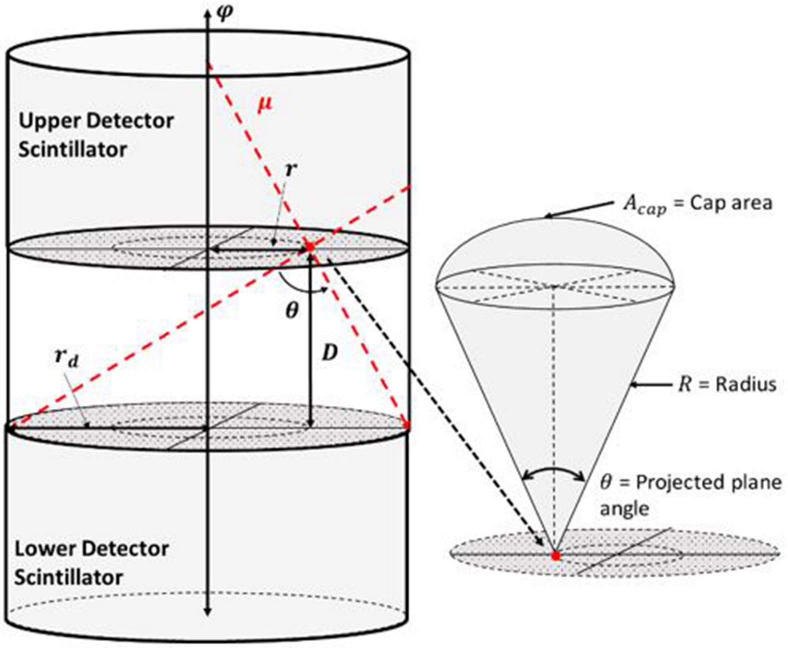

Fig. 1. Schematic diagram of two-fold scintillation muon detector system. Example of cosmic ray muon trajectories (left) and the effective solid angle at one point on the detector surface (right).

that all muons are detected when they traverse detectors regardless of their deposited energy. The projected plane angle in radians is given by

$$\theta(r) = \mathrm{atan}\left(\frac{r_\mathrm{d}+r}{D}\right) + \mathrm{atan}\left(\frac{r_\mathrm{d}-r}{D}\right), \tag{1}$$

where r_d is the radius of detector surface. The area-averaged projected plane angle, θ_avg, and half-projected plane angle, γ, over the detector surface become

$$\theta_\mathrm{avg} = \frac{1}{\pi r_\mathrm{d}^2}\int_{A_\mathrm{d}} r\theta(r)dA_\mathrm{d}, \tag{2}$$

$$\gamma = \frac{\theta_\mathrm{avg}}{2} = \frac{1}{2L}\left[\ln\frac{4L^2+1}{(L^2+1)^2} + \frac{1}{L}\mathrm{atan}(2L) + 2\left(L-\frac{1}{L}\right)\mathrm{atan}\,L\right], \tag{3}$$

$$L \equiv \frac{r_\mathrm{d}}{D}, \tag{4}$$

where A_d is the detector surface area and L is the ratio of r_d to D. Because γ depends on not only r_d but also D, a new parameter, L, is defined. The variance of γ as a function of D for the various detector radii 2.54 cm, 5.08 cm, and 7.62 cm using Eqs. (3) and (4) is shown in Fig. 2. When two detectors are attached, $D = 0$ cm, the half-projected plane angle is 90° regardless of detector radius. On the contrary, it asymptotically approaches 0° as D increases.

The expected muon flux varies within a solid angle that is confined to the detector size and distance. Since the azimuthal angular dependency on the muon flux is insignificant, when the half-plane projected angle is γ, the solid angle is

$$\Omega = 2\pi\int_0^\gamma \sin\phi d\phi. \tag{5}$$

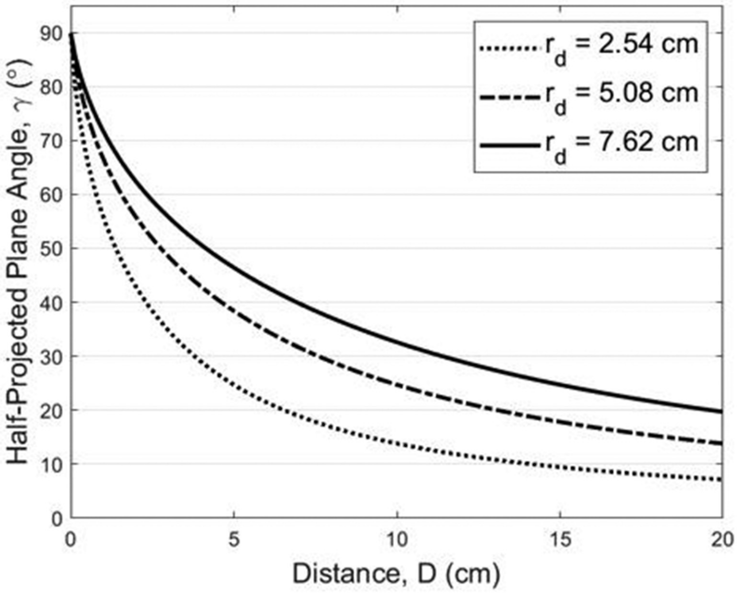

Fig. 2. Half-projected plane angle as a function of detector distance, D, when r_{d} is 2.54 cm, 5.08 cm, and 7.62 cm.

The range of pointing angle of a centerline, φ, extends from 0° to 90°. As the range of pointing angle is uniformly divided by N number of angles,

$$\varphi_i = \frac{\pi i}{2N}\big|_{i=1,\ 2,\ \ldots,\ N}. \tag{6}$$

By integrating the zenith angular dependent cosmic muon flux model, i.e., $I(\varphi)/I_0$ with Eqs. (5) and (6), the effective solid angle over the entire azimuthal angle is given by

$$\Omega'_{\mathrm{eff}}\ (i) = \frac{2\pi}{I_0}\int_{\varphi_i-\gamma}^{\varphi_i+\gamma} I(\phi)\sin\phi d\phi. \tag{7}$$

Because the muon flux is assumed to be invariant over the azimuthal angle, a scaling factor, F, can be expressed by

$$F\ (i) = \frac{A_{\mathrm{cap}}}{A_{2\pi}(i)} = \frac{1-\cos\gamma}{\cos(\varphi_i-\gamma)-\cos(\varphi_i+\gamma)}, \tag{8}$$

where A_{cap} is the cap area shown in Fig. 1 and $A_{2\pi}$ is a circular area between $\varphi \pm \gamma$. The complete effective solid angle equation for the ith zenith angle becomes

$$\Omega_{\mathrm{eff}}\ (i) = \Omega'_{\mathrm{eff}}\ (i)F(i). \tag{9}$$

Since the expected cosmic muon flux is linearly proportional to the effective solid angle, the total muon count rate (CR) is given by

$$CR\ =\ \rho\Omega_{\mathrm{eff}}, \tag{10}$$

where ρ is a conversion constant (muon count rate per steradian). The effective solid angle model as described in Eq. (9) is independent of detector geometry and altitude. It can be solved either analytically or numerically as long as an appropriate intensity, e.g., cosine power or cosine squared, is selected. As an example, using the cosine-squared model, which is the simplest cosmic ray muon flux estimation model, the effective solid angle model (Eqs. (7) and (9)) becomes

$$\Omega'_{\mathrm{eff}}\ (i) = \frac{2\pi}{3}\left[\cos^3(\varphi_i-\gamma)-\cos^3(\varphi_i+\gamma)\right], \tag{11}$$

Table 1 Experimental environments for cosmic ray muon flux measurements.

Date	Location	Elevation
May 2020	40°26′N, 86°54′W	187 m

$$\Omega_{\mathrm{eff}}\ (i) = \left(\frac{2\pi}{3}\right)\ (1-\cos\gamma)[(\cos(\varphi_i-\gamma)+\cos(\varphi_i+\gamma))^2-\cos(\varphi_i-\gamma)\cos(\varphi_i+\gamma)]. \tag{12}$$

The effective solid angle model is publicly available at MATLAB File Exchange [34].

3. Experiment setup

To benchmark the effective solid angle model, we performed a series of cosmic ray muon detection experiments using a two-fold coincidence measurement that consists of two independent scintillation detection systems (details of the experimental environments are summarized in Table 1). In each detection system, a cylindrical sodium iodide scintillation crystal, NaI (Tl), integrated with a photomultiplier tube (PMT) was used to detect cosmic ray muons. The main specifications of the NaI (Tl) crystal and photomultiplier base with preamplifier are summarized in Table 2. The average energy of cosmic ray muons at sea level is 3–4 GeV and the estimated muon energy deposition in the NaI (Tl) crystal using the Bethe equation is approximately 7 MeV cm^{-1} [35]. Although the total energy deposition depends on the muon travel length in the crystal, the average amplitudes of scintillation photon signals are greater than most other background radiation signals. To minimize dead time caused by a long-tailed preamp pulse, we used an amplifier to transform the preamp pulse to a Gaussian-shaped short pulse. The amplifier gain was set as the minimum ($\times 2.5$) in order to efficiently discriminate background noise. The reshaped signals were transmitted to a single channel analyzer with a discriminator level of 10 V (maximum). Because the expected amplitudes of muon signals are greater than 12 V, most background noise signals ($\ll$10 V) are discriminated. To improve the muon detection reliability, we also used a coincidence logic gate which only accepts signals that occur within 500×10^{-9} sec [36]. Using the coincidence measurement technique, we significantly minimized the random noise frequency [37].

4. Monte Carlo simulation

In addition to cosmic ray muon measurements, we performed Monte-Carlo simulations based on the cosine-squared model. Because a trace of a muon trajectory on the detector surface is a random event, the possible interaction points are arbitrarily generated on each detector surface (Fig. 1). The Cartesian coordinates for muon traces on the upper and lower detector surfaces are

$$(x, y, z)_u = (x_m,\ y_m, D)\ \ m = 1,\ 2, \ldots, N, \tag{13}$$

$$(x, y, z)_l = (x_n,\ y_n, 0)\ \ n = 1,\ 2, \ldots, N, \tag{14}$$

where N is the number of muon traces on each detector surface. By connecting two points from the upper (u) and lower (l) surfaces, m and n, the three-dimensional muon trajectories are

Table 2 Selected specifications of NaI (Tl) scintillators, preamps, and PMT [38,39].

	NaI (Tl) crystal	Photomultiplier base with preamplifier	
Model	BICRON 2M2/2	Model	ORTEC276
Density	3.67 g cm^{-3}	PMT stages	10
Yields	~38 000 photons MeV^{-1}	Conversion gain	10^5–10^6
Housing	Aluminum Thickness = 0.508 mm	Output rise/decay time	$t_r < 10^{-7}$ sec $\tau_d \approx 50\ \mu$sec
Dimension	Diameter = 50.8 mm Height = 50.8 mm	Dimension	Diameter = 56 mm Height = 102 mm

reconstructed. The reconstructed angles, $\theta_{\mathrm{m}\to\mathrm{n}}$, and expected muon fluxes, $I_{\mathrm{m}\to\mathrm{n}}$, are

$$\theta_{m\to n} = \arccos\left(\frac{D}{\sqrt{\Delta x^2 + \Delta y^2 + D^2}}\right), \tag{15}$$

$$I_{m\to n} = I_0 \cos^2(\theta_{m\to n}), \tag{16}$$

where $\Delta x = x_{\mathrm{m}} - x_{\mathrm{n}}$ and $\Delta y = y_{\mathrm{m}} - y_{\mathrm{n}}$. The matrices for total reconstructed angles, $\boldsymbol{\Theta}$, and intensities, $\boldsymbol{I}$, are given by

$$\boldsymbol{\Theta} = \begin{bmatrix} \theta_{1\to 1} & \theta_{1\to 2} & \cdots & \theta_{1\to N} \\ \theta_{2\to 1} & \theta_{2\to 2} & & \theta_{2\to N} \\ \vdots & & & \vdots \\ \theta_{N\to 1} & \theta_{N\to 2} & \cdots & \theta_{N\to N} \end{bmatrix}, \tag{17}$$

$$\boldsymbol{I} = \begin{bmatrix} I_{1\to 1} & I_{1\to 2} & \cdots & I_{1\to N} \\ I_{2\to 1} & I_{2\to 2} & & I_{2\to N} \\ \vdots & & & \vdots \\ I_{N\to 1} & I_{N\to 2} & \cdots & I_{N\to N} \end{bmatrix}. \tag{18}$$

The expected muon fluxes at the ith zenith angle, I_{i}, and its mean intensity can be expressed as

$$\boldsymbol{I_i} = I_0 \cos^2(\boldsymbol{\Theta} \pm \varphi_i), \tag{19}$$

$$\bar{\boldsymbol{I}}_{\boldsymbol{i}} = \frac{1}{N^2} \sum \boldsymbol{I_i}. \tag{20}$$

5. Results

To demonstrate the performane of effective solid angle model, we compared it with three results: (i) cosine-squared model, (ii) Monte Carlo simulation, and (iii) experimental measurements. In cosmic ray muon measurement experiments, 21 sets of measurements were performed for seven zenith angles (0°, 15°, 30°, …, 75°, and 90°) and three distances (8 cm, 9.5 cm, and 11 cm) for 24 hours to minimize the day–night flux variation at sea level [40]. The results of muon measurements, estimations by the effective solid angle model, cosine-squared model, PARMA model, and Monte Carlo simulation are summarized in Table 3. The normalized quantities are also included in Table 3 for comparison, and those results are shown in Fig. 3. In addition, a C/E (the ratio of calculated to experimental data) for the measured muon counts for the cosine-squared model, effective solid angle model, PARMA model using EXPACS [30], and Monte Carlo simulation as a function of zenith angles are also shown in Fig. 3. To

Table 3 Experimental data (muon counts per day) and estimations by the effective solid angle model, normalized Monte Carlo simulation results, PARMA model, and cosine-squared model for zenith angles from 0° to 90° when $D = 8$ cm and $r_d = 2.54$ cm [41].

Zenith angle (φ)	Experiment data Counts/day	 Normalized	PARMA [30] Φ_μ/Φ_0	Effective solid angle model Ω_{eff}/Ω_0	Monte Carlo simulation I_i/I_0	$\cos^2\varphi$
0°	1929	1.0000 ± 0.0322	1	1	1.0000 ± 0.1000	1.000
15°	1724	0.8937 ± 0.0296	0.8680	0.9351	0.9368 ± 0.0968	0.933
30°	1472	0.7631 ± 0.0264	0.7836	0.7577	0.7638 ± 0.0874	0.750
45°	1192	0.6179 ± 0.0228	0.5573	0.5154	0.5397 ± 0.0735	0.500
60°	664	0.3442 ± 0.0155	0.3626	0.2731	0.3121 ± 0.0559	0.250
75°	318	0.1649 ± 0.0100	0.1942	0.0957	0.1467 ± 0.0383	0.067
90°	156	0.0809 ± 0.0067	0.0567	0.0615	0.0876 ± 0.0296	0.000

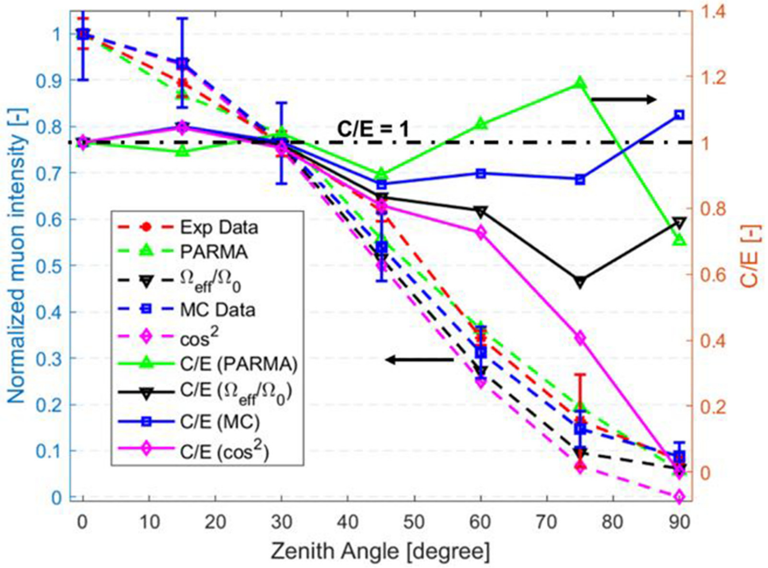

Fig. 3. Comparison of cosmic ray muon measurements and four approaches: (a) effective solid angle model, (b) cosine-squared model, (c) PARMA model, and (d) Monte Carlo simulation (left y-axis) and their C/E (right y-axis) when $D = 8$ cm and $r_d = 2.54$ cm [41].

eliminate the energy dependence, the results generated by EXPACS are integrated over the muon energy (100 MeV to 1 TeV). It is noted that the C/E for the cosine-squared model drops rapidly, especially for high zenith angle levels ($> 60°$), because it assumes no muon is measured when $\varphi = 90°$. On the contrary, the effective solid angle model, PARMA model, and Monte Carlo simulation are in good agreement with the measurements. Although the C/E for effective solid angle model decreases at high zenith angles due to the low muon counts, it provides relatively stable predictions for all zenith angles (C/E > 0.8). The Monte Carlo simulations show the most accurate and stable prediction (C/E = 1.0 ± 0.1). The C/E values for both effective solid angle and PARMA models constantly remain at 1.0 ± 0.15, whereas that of the cosine-squared model decreases from 1 to 0. The mean C/E values for Monte Carlo simulations, effective solid angle, and cosine-squared models when the detector distances are 8 cm, 9.5 cm, and 11 cm, are shown in Fig. 4. The accurate and constant C/E values of effective solid angle model at all distances demonstrate its potential that it can be applied to various detector configurations.

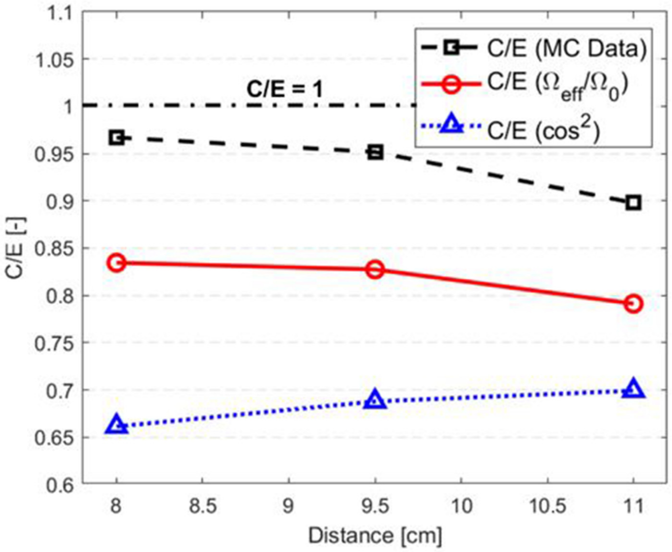

Fig. 4. The mean C/E values as a function of detector distance, D, for three approaches: (a) the effective solid angle model, (b) the cosine-squared model, and (c) the Monte Carlo simulation.

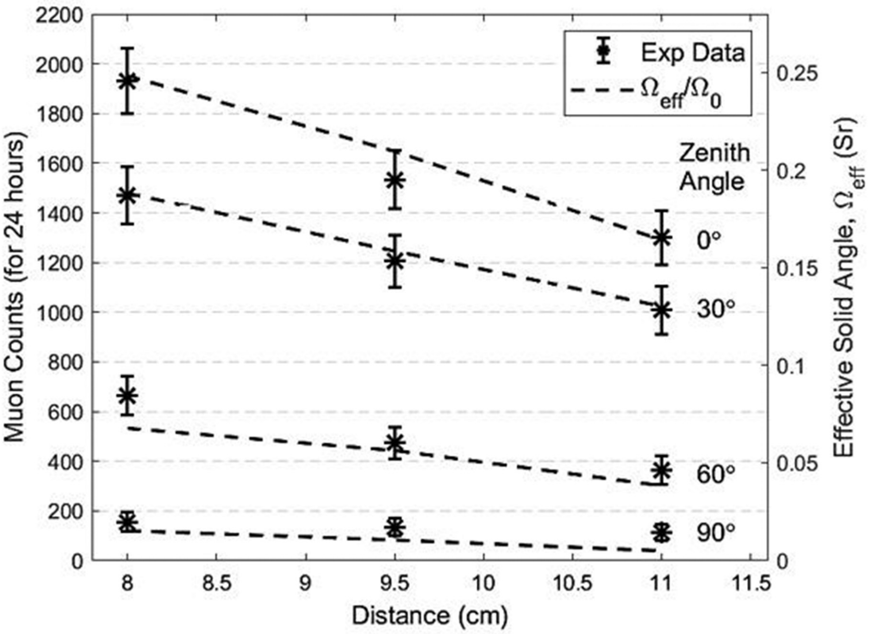

Fig. 5. The effective solid angles as a function of a detector distance, D, for zenith angles, 0°, 30°, 60°, and 90°, and the cosmic muon measurement results (counts for 24 hours). The error bar represents 1σ.

The correlation between daily cosmic muon counts and effective solid angle is shown in Fig. 5. The effective solid angle model accurately estimates the muon counts within a 1σ error level for $\varphi = 0^{\circ}$ and 30°. On the other hand, it does not successfully estimate muon counts within a 1σ error level for $\varphi = 60^{\circ}$ and 90°.

The effective solid angle model as a function of L (Eqs. (3) and (12)) and the measurement data when $r_{\mathrm{d}} = 2.54$ cm and $D = 8$ cm, 9.5 cm, and 11 cm ($L = 0.3175$, 0.2674, and 0.2309, respectively) are shown in Fig. 6. In the range between $L = 0.15$ and 0.4, both the effective solid angle model and the experiment data linearly increase as L increases. Under the conditions

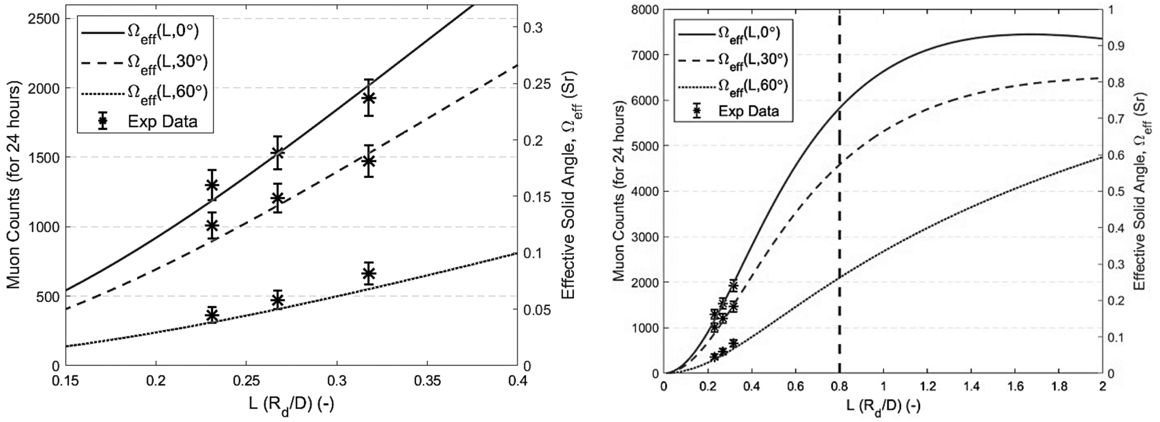

Fig. 6. The effective solid angles as a function of L for zenith angles of 0°, 30°, and 60° when $0.15 < L < 0.4$ (left) and $0 < L < 2.0$ (right). The effective solid angle equation can be simplified to the linear equation when $0.2 < L < 0.8$.

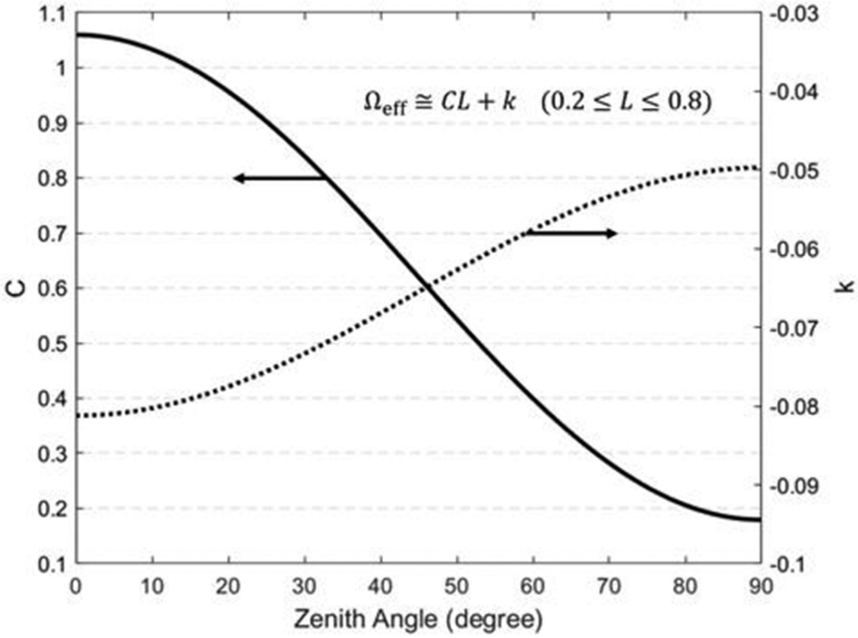

Fig. 7. The constants C and k used in Eq. (22) as functions of the zenith angle when $0.2 < L < 0.8$.

presented in Table 1, the semi-empirical correlation between the effective solid angle and muon count rates per day using the conversion constant, ρ, in Eq. (10) is given by

$$CR \approx 7.52 \times 10^3 \left[\frac{\text{counts/day}}{\text{sr}}\right] \times \Omega_{\text{eff}}\ [\text{sr}], \tag{21}$$

where Ω_{eff} can be found in Eq. (9). Because the effective solid angle linearly increases when $0.2 < L < 0.8$, Eq. (21) can be simplified by

$$CR \approx 7.52 \times 10^3 \times (CL + k). \tag{22}$$

The constants, C and k, as functions of the zenith angle, are shown in Fig. 7 and summarized in Table 4 for selected zenith angles.

Table 4 The constants C and k used in Eq. (22) for selected zenith angles when $0.2 < L < 0.8$.

Zenith angles	C	k
0^o	1.0599	−0.0812
15^o	1.0009	−0.0791
30^o	0.8398	−0.0733
45^o	0.6197	−0.0654
60^o	0.3995	−0.0576
75^o	0.2384	−0.0518
90^o	0.1794	−0.0497

5. Conclusion

A new semi-empirical approach, the effective solid angle model, is developed to predict the cosmic ray muon flux at all zenith angles. By integrating the three-dimensional geometric characteristic of muon detector into a simple model (e.g., cosine-squared model), the effective solid angle model successfully estimates the cosmic ray muon count rates at all zenith angles. The performance of effective solid angle model is compared with experimental measurements and we demonstrate that the mean C/E level is improved from 0.7 for the cosine-squared model to 0.95 for the effective solid angle model when $D = 9.5$ cm. It is worth noting that a new semi-empirical effective solid angle model, despite its simplicity, is versatile enough to account for all detector geometries and configurations. The results can be improved by using a more advanced model such as PARMA instead of the cosine-squared model. The effective solid angle depends on two variables, detector surface radius and distance, and they are combined by introducing a new parameter, L, which is the ratio of the radius to the distance. The effective solid angle model as a function of L shows a linearity in $0.2 < L < 0.8$ for all zenith angles. In addition, a semi-empirical conversion equation is presented so that the effective solid angle is converted to the cosmic ray muon count rate. The improved model for estimating the cosmic ray muon flux for all detection conditions is especially significant for high zenith angles ($> 60^o$) because the cosine-squared model is limited in use for low zenith angles due to the large uncertainties. We anticipate our results to improve modeling quality in muon radiographic and monitoring applications by maximizing the utilizability of cosmic ray muons.

Conflict of interest

The authors declare no competing interests.

Acknowledgments

This work was supported by the Purdue University Research Foundation.

References

[1] B. Rossi, Cosmic Rays (McGraw-Hill, New York, 1964).
[2] S. Chatzidakis et al., Proc. Int. Conf. Nuclear Plant Instrumentation, Control, and Human–Machine Interface Technologies, p. 237 (2017).
[3] S. Chatzidakis, C. K. Choi, and L. H. Tsoukalas, Nucl. Inst. Meth. Phys. Res. A **828**, 37 (2016).
[4] G. Jonkmans, V. N. P. Anghel, C. Jewett et al., Ann. Nucl. Energy **53**, 267 (2013).
[5] D. Poulson et al., Nucl. Inst. Meth. Phys. Res. A **842**, 48 (2017).
[6] S. Chatzidakis, C. K. Choi, and L. H. Tsoukalas, IEEE Trans. Nucl. Sci. **63**, 2866 (2016).

[7] S. Chatzidakis, C. K. Choi, and L. H. Tsoukalas, Trans. Am. Nucl. Soc. **114**, 152 (2016). https://inis.iaea.org/search/search.aspx?orig_q=RN:52032095
[8] J. Bae and S. Chatzidakis, INMM/ESARDA Jt. Annu. Meet, **a411**
[9] O. Kamaev, E. T. Rand, B. M. Van Der Ende et al., Nucl. Inst. Methods Phys. Res. A **944**, 162503 (2019).
[10] V. Anghel et al., Proc. IEEE Nuclear Science Symp. and Medical Imaging Conf., p. 547 (2010).
[11] K. Gnanvo et al., Proc. IEEE Nuclear Science Symp. and Medical Imaging Conf., p. 552 (2010).
[12] K. Gnanvo, L. V Grasso, M. Hohlmann et al., Nucl. Inst. Meth. Phys. Res. A **652**, 16 (2011).
[13] S. Pesente et al., Nucl. Inst. Meth. Phys. Res. A **604**, 738 (2009).
[14] L. J. Schultz, K. N. Borozdin, J. J. Gomez et al., Nucl. Instr. Meth. Phys. Res. A **519**, 687 (2004).
[15] M. Hohlmann et al., IEEE Trans. Nucl. Sci. **56**, 1356 (2009).
[16] D. Schouten and P. Ledru, J. Geophys. Res. Solid Earth **123**, 8637 (2018).
[17] E. Guardincerri et al., Pure Appl. Geophys. **174**, 2133 (2017).
[18] S. Buontempo et al., Earth, Planets, Space **62**, 131 (2010).
[19] L. Del Santo et al., Nucl. Part. Phys. Proc. **291–293**, 122 (2017).
[20] D. Schouten, Phil. Trans. R. Soc. A **377**, 20180061 (2018).
[21] J. Bae and S. Chatzidakis, Trans. Am. Nucl. Soc. **125**, 400 (2021). https://arxiv.org/ftp/arxiv/papers/2201/2201.02591.pdf
[22] A. Erlandson, K. Boniface, V. N. P. Anghel et al., CNL Nucl. Rev. **7**, 1 (2018).
[23] P. Checchia et al., Phil. Trans. R. Soc. A **377**, 20180065 (2019).
[24] J. Bae and S. Chatzidakis, Sci. Rep. **12**, 2559 (2022).
[25] T. K. Gaisser, R. Engel, and E. Resconi, Cosmic Rays and Particle Physics (Cambridge University Press, Cambridge, 2016).
[26] C. L. Morris et al., Nucl. Inst. Meth. Phys. Res. B **330**, 42 (2014).
[27] H. K. M. Tanaka, K. Nagamine, S. N. Nakamura et al., Nucl. Inst. Meth. Phys. Res. A **555**, 164 (2005).
[28] T. Sato, PLoS One **10**, e0144679 (2015).
[29] T. Sato, H. Yasuda, K. Niita et al., Radiat. Res. **170**, 244 (2008).
[30] T. Sato, PLoS One **11**, e0160390 (2016).
[31] M. Bahmanabadi, Nucl. Inst. Meth. Phys. Res. A **916**, 1 (2019).
[32] J. L. Autran, D. Munteanu, T. S. Saoud et al., Nucl. Inst. Meth. Phys. Res. A **903**, 77 (2018).
[33] I. M. Brancus et al., Nucl. Phys. B **176**, 370 (2008).
[34] J. Bae, Effective Solid Angle for Cosmic Muon Flux Estimation (MATLAB Central File Exchange, Natick, MA, 2021) (available at: https://www.mathworks.com/matlabcentral/fileexchange/100806-effective-solid-angle-for-cosmic-muon-flux-estimation, date last accessed February 2, 2022).
[35] P. A. Zyla et al. [Particle Data Group], Prog. Theor. Exp. Phys. **2020**, 083C01 (2020).
[36] AMETEK Inc., DSPEC 50® and DSPEC 502® Digital Gamma-Ray Spectrometer User's Manual (2018).
[37] D. M. Lowder, T. Miller, P. B. Price et al., Nature **353**, 331 (1991).
[38] ORTEC, Model 276 Photomultiplier Base Operating and Service Manual (2005).
[39] Saint-Gobain Crystals, Integrated Scintillation Detectors (2018).
[40] H. M. Mok and K. M. Cheng, arXiv:physics/0105005 [Search inSPIRE].
[41] J. Bae, S. Chatzidakis, and R. Bean, Proc. 28th Int. Conf. Nuclear Engineering, Vol. 4 (2021).